Investigation of AC Copper Loss Considering Effect of Field and Armature Excitation on IPMSM With Hairpin Winding

Soo-Hwan Park, Jun-Woo Chin, Kyoung-Soo Cha, Jun-Yeol Ryu, and Myung-Seop Lim, *Member, IEEE*

***Abstract*—As the torque density of traction motors for electric vehicles (EVs) increases, winding technology with a large conductor area, such as hairpin winding, is widely used. However, it has a disadvantage of large AC copper loss affected by the skin and proximity effect. Therefore, the AC copper loss should be considered for deriving characteristics of interior permanent magnet synchronous motors (IPMSMs). This article deals with the maximum torque per ampere (MTPA) and flux-weakening control characteristics of the IPMSM considering AC copper loss. As the AC copper loss is caused by armature and field excitation, a separation process of AC copper loss by each cause is proposed. By using the process, the separated AC copper loss can be analyzed according to the current vector and rotational speed. However, it is inefficient to calculate the AC copper loss according to rotational speed using transient analysis. Therefore, a computationally efficient method of calculating AC copper loss based on magneto-static analysis is presented. In addition, advanced *d, q*-axis equivalent model considering AC copper loss is proposed to analyze MTPA and flux-weakening control characteristics of IPMSM. By using the proposed *d, q*-axis equivalent model, the IPMSM can be designed considering the AC copper loss efficiently and accurately.**

***Index Terms*—AC copper loss, flux-weakening control, hairpin windings, interior permanent magnet synchronous motor, maximum torque per ampere (MTPA).**

Manuscript received 21 April 2022; revised 5 September 2022 and 14 November 2022; accepted 21 December 2022. Date of publication 9 January 2023; date of current version 9 June 2023. This work was supported by the National Research Foundation of Korea funded by the Korea government (Ministry of Science, ICT & Future Planning) under Grant 2018R1C1B5085447. *(Corresponding author: Myung-Seop Lim.)*

Soo-Hwan Park is with the R&D Division, Hyundai Motor Company, Hwaseong 18280, South Korea, and also with the Department of Automotive Engineering, Hanyang University, Seoul 04763, South Korea (e-mail: park.sh@hyundai.com).

Jun-Woo Chin is with the Future Powertrain Technologies Research Laboratory of Korea Automotive Technology Institute (KATECH), Cheonan 31214, South Korea, and also with the Department of Automotive Engineering, Hanyang University, Seoul 04763, South Korea (e-mail: jwchin@katech.re.kr).

Kyoung-Soo Cha is with the Korea Institute of Industrial Technology, Daegu 42994, South Korea, and also with the Department of Automotive Engineering, Hanyang University, Seoul 04763, South Korea (e-mail: kscha@kitech.re.kr).

Jun-Yeol Ryu and Myung-Seop Lim are with the Department of Automotive Engineering, Hanyang University, Seoul 04763, South Korea (e-mail: jesus0925@hanyang.ac.kr; myungseop@hanyang.ac.kr).

Color versions of one or more figures in this article are available at https://doi.org/10.1109/TIE.2023.3234154.

Digital Object Identifier 10.1109/TIE.2023.3234154

I. Introduction

INTERIOR permanent magnet synchronous motors (IPMSMs) are widely used in automotive industry because of its suitable characteristics for high-speed trend in electric powertrain (e-powertrain) and its strong flux-weakening characteristics due to high saliency rotor structure [1]. The competitiveness of electric vehicles (EVs) is its mileage, and the improvement of mileage can be achieved by improving the energy density of battery or enhancing capacity of battery, or reducing the power loss of e-powertrain [2], [3]. However, improving the performance of battery requires a huge cost, and enhancing the capacity of battery increases the weight and price of vehicle. Therefore, the most effective method for improving the mileage is to increase the efficiency of e-powertrain.

The e-powertrain consists of DC–DC converter, inverter, traction motor, and the reducer [4], [5]. Thus, the mileage of EVs is affected by the electromagnetic and mechanical loss of e-powertrain [6]. Among the components of the e-powertrain, the traction motor consumes large proportion in the power loss [7]. The competitiveness of the traction motor is determined by its high power density and high efficiency. However, the two factors have a trade-off relationship because the high power density is proportional to the current density and the high current density causes high copper loss [8], [9]. Therefore, winding technology with high fill factor such as hairpin windings has been widely adopted to achieve the high efficiency with high power density [5], [10].

The hairpin windings have advantages such as low DC resistance, large contact area for heat dissipation, high productivity, and high current capacity [11], [12]. However, the AC copper loss should be considered when designing the IPMSMs with hairpin windings. The AC copper loss is affected by the skin and proximity effect by the armature current and the eddy current induced by the field flux [13], [14], [15]. Therefore, the AC copper loss has nonlinear characteristics according to the current vector and its frequency [13], [14]. There are three main ways to calculate the AC copper loss.

The first method is an analytical method that considers the slot leakage flux and skin depth according to the winding position. In [16], an analytical method for calculating AC resistance for rectangular shape slot with formed winding was proposed. A method of calculating the AC resistance considering the skin/proximity effect by analytically calculating the slot leakage flux when a current flows through the armature winding is presented. Wu et al. [17] proposed a simplified analytical model for calculating open-circuit AC copper loss. Using the proposed method, the trend of open-circuit AC copper loss for various design parameters can be analyzed. The analytical method is suitable for analyzing the trend of AC copper loss according to design variables, but it has a disadvantage in that it is difficult to accurately calculate the AC copper loss when a complex magnetic circuit is applied and the effect of magnetic saturation.

The second method is to calculate the AC copper loss using finite element analysis (FEA). FEA has an advantage of being able to derive AC copper loss by accurately calculating the leakage flux and skin/proximity effect of complex magnetic circuits such as electric machines. In [15], the trend of AC/DC-ratio according to the current density and various types of electric machine was analyzed using FEA and analytical method. Bardalai et al. [18] proposed a method placing conductors in slot for minimizing AC copper loss. In order to calculate the AC copper loss according to the position of conductors, FEA was used to calculate the accurate AC copper loss. The transient analysis of AC copper loss using FEA is also widely used in the development of high fill factor winding technology to improve efficiency [19]. However, the calculation of AC copper loss has the disadvantage that it requires high computation cost because transient analysis is necessary. The following study is a case of calculating AC copper loss using FEA.

The last method is a hybrid method that utilizes the advantages of FEA and analytical method. By combining the FEA which has high accuracy FEA and analytical method which has low computation cost, relatively accurate AC copper loss can be derived faster than using transient analysis. Chin et al. [20] proposed a post-processing method using vector potential derived from magneto-static analysis. As a result of combining FEA and analytical method, it is possible to calculate AC copper loss with low computation cost considering the effect of permanent magnets (PMs). Taran et al.[21] proposed a hybrid method for efficient calculation of AC copper loss for an axial-flux machine. The proposed method calculates the magnetic flux density with relatively fast and high accuracy by adjusting the mesh of the 3-D winding, and the eddy current loss can be calculated using the magnetic flux density and analytical method. In addition, since the AC copper loss is affected by the slot leakage flux, a method for calculating the AC copper loss by mapping the calculated slot leakage flux using nonlinear FEA to the winding shape has been proposed [22]. As we have seen those studies, it is necessary to accurately calculate the nonlinear AC copper loss to accurately predict the characteristics of the traction motor. Therefore, the hybrid method is used in this study to consider the AC copper loss in calculating current vector control characteristics of IPMSMs.

It is important to analyze the characteristics of IPMSMs considering the AC copper loss as much as efficiently calculating the AC copper loss. In order to consider the AC copper loss in the *d, q*-axis model, the AC copper loss should be converted into an AC resistance. The AC resistance has been derived using the AC copper loss calculated with both field and armature excitation [23], [24]. The converted AC resistance is used as a nonlinear parameter along with *d, q*-axis inductances, flux-linkage, and iron loss to calculate the characteristics of maximum torque per ampere (MTPA) and flux-weakening control [13], [14]. However, the AC copper loss includes eddy current loss due to skin and proximity effect by fluctuation of slot leakage flux [25]. Accordingly, the effect of field excitation causes eddy current loss in the conductors even under no-load condition. Therefore, it is necessary to propose a proper method to consider the AC copper loss in analyzing the characteristics of IPMSMs.

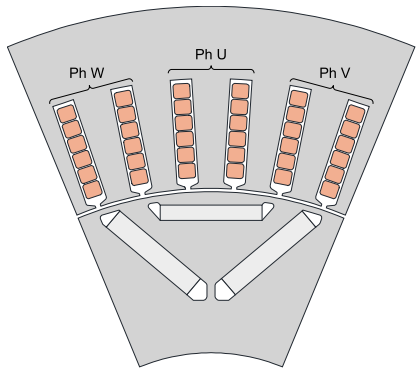

Fig. 1. Target IPMSM for EV traction with hairpin windings.

This article proposes a strategy for deriving MTPA and flux-weakening characteristics of IPMSMs considering the effect of AC copper loss. The contributions of this article are as follows. The effect of AC copper loss caused by field and armature excitation on the characteristics of IPMSMs is analyzed. The separation method for each component of AC copper loss and advanced *d, q*-axis voltage equations for characteristics calculation are proposed. Using the proposed separation method and equivalent circuits, it is possible to calculate the characteristics of IPMSMs with high AC copper loss such as traction motor more accurately.

II. Analysis of AC Copper Loss for IPMSM

Fig. 1 shows the target IPMSM for EV traction. Since the torque density is important in EV traction, the IPMSM is designed using hairpin windings. The specifications of the IPMSM are listed in Table I. The target motor has 8-poles and 48-slots with six conductors per slot. Fig. 2 shows the MTPA and flux-weakening control regions of the target motor. Before the voltage limit curve, the current vector is determined under MTPA control, and the flux-weakening control is additionally applied after the curve.

A. Causes of AC Copper Loss

The AC copper loss is caused by the skin and proximity effect due to the fluctuation of external magnetic field that means the

TABLE I
SPECIFICATIONS OF 8-POLES 48-SLOTS IPMSM FOR EV TRACTION

Item	Unit	Value
Number of poles	–	8
Number of slots	–	48
DC link voltage	V	350
Max. output power	kW	115
Peak torque	N·m	290
Max. speed	rpm	12 000
Peak current	A_{rms}	365
Operating temperature	°C	100
Conductors per slot	–	6

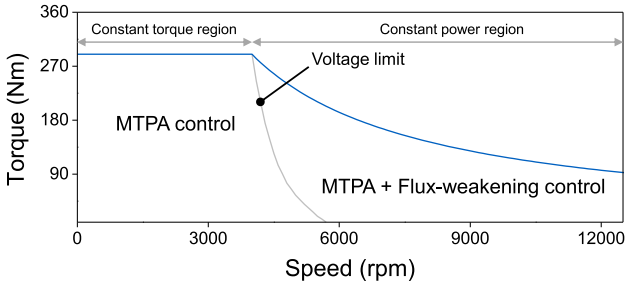

Fig. 2. MTPA and flux-weakening control regions of IPMSM.

slot leakage flux caused by magnetic saturation. The slot leakage flux is affected by the armature and the field excitation acting as the magnetomotive force (MMF) of the magnetic circuit. Therefore, the AC copper loss consists of AC copper loss due to the armature and field excitation as

$$W_{\mathrm{AC}} = W_{\mathrm{AC},a} + W_{\mathrm{AC},f} \tag{1}$$

where W_{AC} is the total AC copper loss; $W_{\mathrm{AC},a}$ and $W_{\mathrm{AC},f}$ are the AC copper loss caused by armature and field excitation; Since the AC copper loss is a superposition of DC copper loss and eddy current loss in conductors, the DC copper loss is included in $W_{\mathrm{AC},a}$.

Various methods have been proposed for efficient calculation of AC copper loss [9], [22], but we adopt the magneto-static analysis-based postprocessing method to analyze the AC copper loss by each cause accurately [20]. The AC copper loss has nonlinear characteristics according to the magnetic saturation and frequency, and the calculation of eddy current is required to derive the AC copper loss. Therefore, a large amount of transient analysis is necessary to mapping the AC copper loss. By using the magneto-static analysis-based postprocessing method, computing power can be reduced by calculating AC copper loss at the same time as calculating inductance, flux-linkage, and iron loss. The method calculates the AC copper loss using the magnetic vector potential, $\mathbf{A}$, computed with the magneto-static analysis. The method is effective in computing time than the transient analysis because the AC copper loss can be calculated by scaling the synchronous frequency due to the magneto-static analysis. In addition, the calculated AC copper loss can be used for characteristic analysis using *d, q*-axis equivalent circuits because it is a function of the magnetization current vector and frequency. The magnetic vector potential calculated using magneto-static analysis can be used when calculating the AC copper loss assuming that the magnetic field generated by the eddy current can be negligible compared to the main magnetic field. The governing equation for magneto-static analysis with PMs is expressed as

$$\nabla \times \left[\frac{1}{\mu}(\nabla \times \mathbf{A})\right] = \mathbf{J_0} + \mathbf{J_m} \tag{2}$$

where μ is the magnetic permeability; $\mathbf{J_0}$ and $\mathbf{J_m}$ are the armature current density and equivalent magnetizing current density, respectively; Then, the electric field intensity that causes the eddy current in the conductors can be computed using the Faraday's law as

$$\nabla \times \mathbf{E_e} = -\frac{\partial \mathbf{B}}{\partial t} = -\frac{\partial (\nabla \times \mathbf{A})}{\partial t} \tag{3}$$

where $\mathbf{E_e}$ and $\mathbf{B}$ are the electric field intensity and magnetic flux density, respectively; Therefore, the time dependent eddy current density for conductors, $\mathbf{J_e}$, can be derived as

$$\mathbf{J_e} = \sigma \mathbf{E_e} = \sigma \frac{\partial \mathbf{A}}{\partial t} \tag{4}$$

where σ is the conductivity of conductors; A practical method to calculate AC copper loss from the results of finite element analysis is presented as follows.

As the eddy current density represents only the eddy current without considering the instantaneous input current, it is necessary to calculate the current distribution in the conductors including the input current. Since the input current is a known value according to the given condition, the actual current density considering both the input current and eddy current for each element can be expressed as

$$J_0^{i,j}(t) = J_e^{i,j}(t) + \left(\frac{I_0(t)}{N_p} - \sum_{m=1}^{N_e} J_e^{i,m}(t) \cdot S^{i,m}\right) \Big/ \sum_{m=1}^{N_e} S^{i,m} \tag{5}$$

where $J_0^{i,j}$ and $J_e^{i,j}$ is the actual current density and eddy current density for conductor i and element j, respectively; I_0 is the instantaneous input current; N_p is the parallel circuit; S is the area of element; N_e is the number of elements; Finally, the AC copper loss can be calculated as

$$W_{\mathrm{AC}}(t) = \sum_{n=1}^{N_c} \sum_{m=1}^{N_e} \left(J_0^{n,m}(t)\right)^2 \cdot S^{n,m} \cdot L_{stk} \tag{6}$$

where L_{stk} is the stack length of core material; N_c is the number of conductors.

Fig. 3 shows the comparison of AC copper loss derived using transient FEA and proposed method according to the electrical angle. The comparison was carried out from conductor indexed by 1 which is closest to the air-gap through the conductor indexed by 5 which is furthest away from the air-gap. As a result of using the magnetic vector potential calculated using FEA, the method can calculate the AC copper loss accurately. Since the conductor

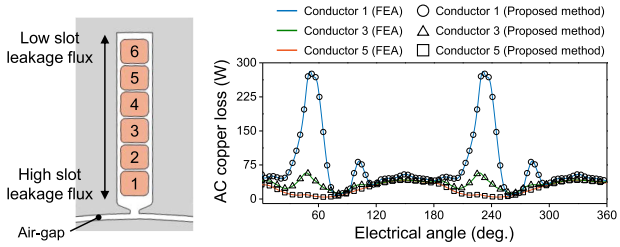

Fig. 3. Comparison of AC copper loss derived using transient FEA and proposed method according to the conductor position.

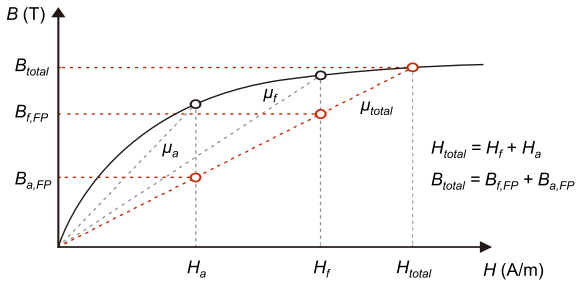

Fig. 4. Principle of frozen permeability method for separating AC copper loss.

1 is located close to the air-gap, the change in slot leakage flux is large, so the change in AC copper loss according to the rotor position is large. On the other hand, the change in AC copper loss due to armature excitation is dominant in conductor 5 because it is located far from the air-gap and the fluctuation of the slot leakage flux is small.

To emphasize that the proposed method is advantageous in terms of computing time, a comparison of computing time for magneto-static analysis-based and transient analysis-based method was conducted. The comparison was performed using a computer with a CPU of Intel Core i7-10700 k and RAM of 32 GB. The FEA solver of JMAG was used for the comparison, and the number of elements for FEA model was 17 873. The AC copper loss was calculated under the same conditions as the analysis of Fig. 3, and it took 63 s to calculate the AC copper loss using the magneto-static analysis-based method. However, as a result of using the transient analysis, it took 169 s to derive the AC copper loss. This is because the AC copper loss should be derived after the eddy current reaches the steady-state. Therefore, the transient analysis should be performed 2 electrical period.

B. Separation of AC Copper Loss Using Frozen Permeability Method

Since the AC copper loss is caused by the influence of field and armature excitation, it is necessary to separate the AC copper loss by component to analyze the AC copper loss. This section deals with the separation of the AC copper loss using the frozen permeability (FP) method. The principle of the FP method is shown in Fig. 4 [26]. By using the FP method, the magnetic vector potential can be calculated when only the field or armature

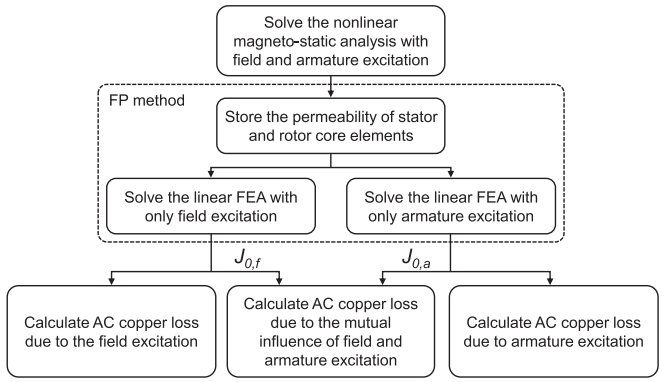

Fig. 5. Flowchart for separating AC copper loss using frozen permeability method.

is excited after fixing the permeability of each element in a state where the entire MMF is excited.

Fig. 5 shows the flowchart for separating of the AC copper loss using FP method [27]. After the nonlinear magneto-static analysis is performed, the FP method and post-processing are conducted to separate the AC copper loss when only each MMF is excited. Then, the AC copper loss according to the mutual influence of both MMF can be calculated using the actual current density for each MMF component.

The calculated actual current density using the magnetic vector potential and (2) through (5) can be separated as

$$\mathbf{J_0} = \mathbf{J_{0,f}} + \mathbf{J_{0,a}} \tag{7}$$

where $\mathbf{J_{0,f}}$ and $\mathbf{J_{0,a}}$ are the actual current density when the field or armature is excited only, respectively; Then, the AC copper loss can be expressed as follows by substituting (7) into (6).

$$W_{\mathrm{AC}}(t) = \sum_{n=1}^{N_c}\sum_{m=1}^{N_e}\left(J_{0,f}^{n,m}(t) + J_{0,a}^{n,m}(t)\right)^2 S^{n,m} L_{stk}. \tag{8}$$

Therefore, the AC copper loss can be separated into terms due to armature and field excitation as

$$W_{\mathrm{AC}}(t) = \underbrace{\sum_{n=1}^{N_c}\sum_{m=1}^{N_e}\left(J_{0,a}^{n,m}(t)\right)^2 S^{n,m} L_{stk}}_{\text{AC copper loss due to armature excitation}} + \underbrace{\sum_{n=1}^{N_c}\sum_{m=1}^{N_e}\left(J_{0,f}^{n,m}(t) + 2J_{0,f}^{n,m}(t)J_{0,a}^{n,m}(t)\right)^2 S^{n,m} L_{stk}}_{\text{AC copper loss due to field excitation}}. \tag{9}$$

In this equation, the current density due to each MMF change according to the armature loading and magnetic loading and current vector control. Therefore, the AC resistance of the equivalent circuit and the equivalent resistance for eddy current loss are also factors that change with torque and speed. The AC copper loss due to field excitation is equivalent to the second term in (9), which in influenced by the current density due to the field excitation.

Fig. 6(a)–(d) shows the waveform of AC copper loss according to the current vector and rotational speed. It can be seen that the AC copper loss due to armature excitation increases as

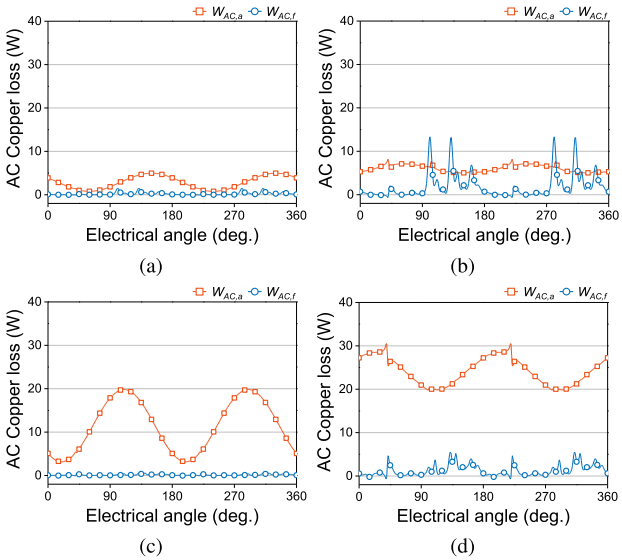

Fig. 6. Waveform of AC copper loss by component according to current vector and rotational speed: (a) $i_e = 20$ A_{rms}, $\beta = 30°$, $\omega_m = 3000$ rpm, (b) $i_e = 20$ A_{rms}, $\beta = 30°$, $\omega_m = 9000$ rpm, (c) $i_e = 40$ A_{rms}, $\beta = 70°$, $\omega_m = 3000$ rpm, (d) $i_e = 40$ A_{rms}, $\beta = 70°$, $\omega_m = 9000$ rpm.

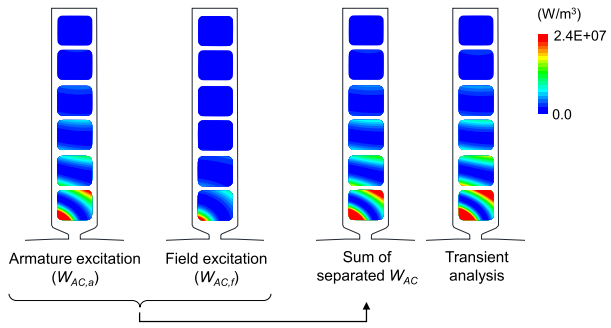

Fig. 7. Comparison of the sum of each component of the AC copper loss calculated based on magneto-static analysis and the AC copper loss calculated using transient analysis.

the amplitude of current vector and rotational speed increases. However, the AC copper loss due to field excitation increases as the rotational speed increases. Although the armature excitation in Fig. 6(d) is increased compared to that in Fig. 6(b), the eddy current loss is decreased because the field excitation is decreased due to the flux-weakening effect as the d-axis current increases.

In order to analyze the AC copper loss for each conductor position, the AC copper loss density should be derived. The AC copper loss density for each component can be calculated by dividing the volume per element by both sides in (9) as

$$W_{AC,a}^{n,m}(t) = \left(J_{0,a}^{n,m}(t)\right)^2 \tag{10}$$

$$W_{AC,f}^{n,m}(t) = \left(J_{0,f}^{n,m}(t)\right)^2 + 2J_{0,f}^{n,m}(t) \cdot J_{0,a}^{n,m}(t). \tag{11}$$

Fig. 7 compares the sum of each component of the AC copper loss density calculated based on magneto-static analysis and the AC copper loss density calculated using transient analysis. The difference between the proposed method and transient analysis

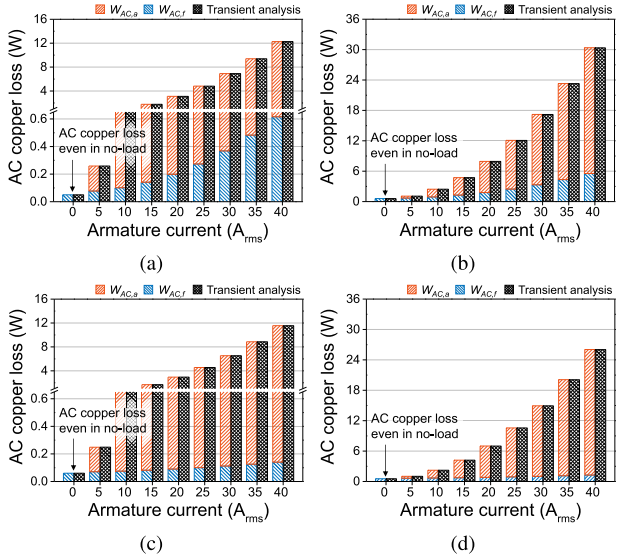

Fig. 8. AC copper loss by component according to current vector and rotational speed: (a) $\omega_m = 3000$ rpm, $\beta = 30°$, (b) $\omega_m = 3000$ rpm, $\beta = 70°$, (c) $\omega_m = 9000$ rpm, $\beta = 30°$, (d) $\omega_m = 9000$ rpm, $\beta = 70°$.

is due to whether the eddy current is considered. It can be seen that the result of summing the AC copper loss density of each component is same as the calculated AC copper loss density with both armature and field excited. Fig. 8(a)–(d) shows the comparison between the AC copper loss calculated using magneto-static analysis and transient analysis according to the current vector and rotational speed. As a result of comparing the sum of the separated AC copper loss and the calculated using transient FEA, it can be seen that the nonlinear AC copper loss according to the current vector and rotational speed is calculated properly. Therefore, the proposed separation method of AC copper loss is reasonable.

The MTPA and flux-weakening control considering AC copper loss can be achieved by utilizing the AC copper loss as an AC resistance. The AC resistance is calculated by dividing the AC copper loss by the square of the current. However, when the AC resistance is calculated using the total AC copper loss, the AC resistance diverges because there is an AC copper loss due to the field excitation even if the armature current converges to zero as shown in Fig. 8(a)–(d). Therefore, we propose a process for considering each AC copper loss into d, q-axis model of IPMSM shown in following section.

III. MTPA and Flux-Weakening Characteristics of IPMSM Considering AC Copper Loss

A. Mathematical Model of IPMSM Considering AC Copper Loss

In order to analyze the characteristics of the IPMSM according to the current vector, a mathematical model of the IPMSM considering the AC copper loss should be derived. The proposed d, q-axis model considering AC copper loss is shown in Fig. 9. The AC copper loss due to armature excitation is considered as AC resistance and the AC copper loss due to field excitation is considered as equivalent resistance in the proposed model. In

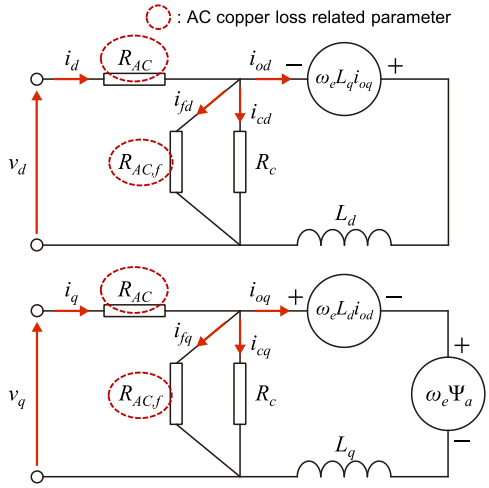

Fig. 9. Proposed *d*, *q*-axis model for IPMSM considering AC copper loss.

this article, the eddy current loss of PMs and mechanical loss are not considered in the *d*, *q*-axis model. Then, the mathematical model of IPMSM in a steady-state can be expressed as

$$\begin{bmatrix} v_d \\ v_q \end{bmatrix} = R_{\mathrm{AC},a} \begin{bmatrix} i_d \\ i_q \end{bmatrix} + \left(1 + \frac{(R_c + R_{\mathrm{AC},f})\, R_{\mathrm{AC},a}}{R_c R_{\mathrm{AC},f}}\right) \begin{bmatrix} v_{od} \\ v_{oq} \end{bmatrix} \tag{12}$$

$$\begin{bmatrix} v_{od} \\ v_{oq} \end{bmatrix} = \begin{bmatrix} 0 & -\omega_e L_q \\ \omega_e L_d & 0 \end{bmatrix} \begin{bmatrix} i_{od} \\ i_{oq} \end{bmatrix} + \begin{bmatrix} 0 \\ \omega_e \psi_a \end{bmatrix} \tag{13}$$

$$R_c = \frac{v_{od}^2 + v_{oq}^2}{W_c} \quad R_{\mathrm{AC},f} = \frac{v_{od}^2 + v_{oq}^2}{W_{\mathrm{AC},f}} \tag{14}$$

$$i_{cd} = -\frac{v_{od}}{R_c} \quad i_{cq} = \frac{v_{oq}}{R_c} \quad i_{fd} = -\frac{v_{od}}{R_{\mathrm{AC},f}} \quad i_{fq} = \frac{v_{oq}}{R_{\mathrm{AC},f}} \tag{15}$$

where the subscripts of *d* and *q* are the *d*, *q*-axis; v_d and v_q are the terminal voltages; v_{od} and v_{oq} are the induced voltages; i_{od} and i_{oq} are the magnetization currents; R_{AC} is the AC resistance per phase; L_d and L_q are the *d*, *q*-axis inductance; ψ_a is the flux-linkage by PMs; ω_e is the electrical rotational speed; W_c is the iron loss; R_c and R_f are the equivalent resistance for iron loss and AC copper loss due to field excitation, respectively; and the i_{cd}, i_{cq}, i_{fd}, i_{fq} are the *d*, *q*-axis currents for iron loss, and eddy current loss, respectively; Then, the electromagnetic torque and *d*, *q*-axis currents can be calculated as

$$T_e = 1.5 P_n \left\{\psi_a i_{oq} + (L_d - L_q)\, i_{od} i_{oq}\right\} \tag{16}$$

$$i_d = i_{od} + i_{cd} + i_{fd} \quad i_q = i_{oq} + i_{cq} + i_{fq} \tag{17}$$

where i_d and i_q are the *d*, *q*-axis currents; Finally, the AC resistance per phase can be expressed as follows:

$$R_{\mathrm{AC},a} = \frac{W_{\mathrm{AC},a}/n_s}{\sqrt{\left(i_d^2 + i_q^2\right)/2}} + R_{\mathrm{end}} \tag{18}$$

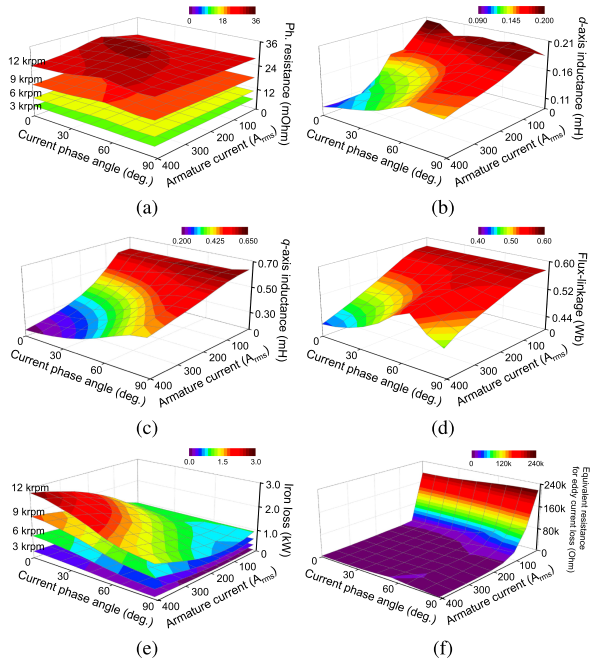

Fig. 10. Nonlinear motor parameters of IPMSM according to current vector: (a) AC resistance, (b) *d*-axis inductance, (c) *q*-axis inductance, (d) flux-linkage, (e) iron loss, and (f) equivalent resistance for AC copper loss due to field excitation at 12 000 rpm.

where n_s is the number of phases; R_{end} is the DC resistance of end winding; The resistance of end winding is assumed as the DC resistance because the magnetic flux variation due to the external magnetic field is small [28].

B. MTPA and Flux-Weakening Characteristics of IPMSM

In this section, the MTPA and flux-weakening control characteristics of IPMSM derived using the proposed *d*, *q*-axis model are analyzed. Fig. 10(a)–(f) shows the motor parameters of the IPMSM according to the current vector and rotational speed. As the magnetic saturation of the stator and rotor core varies according to the current vector, the motor parameters have nonlinear characteristics. It can be seen that the equivalent resistance for eddy current loss is diverged infinitely when the eddy current loss of conductors is small. In the conventional model, characteristics of the IPMSM are calculated using DC resistance, *d*, *q*-axis inductances, flux-linkage, and iron loss presented in Fig. 10(b)–(e). On the other hand, the characteristics derived using the proposed model are calculated by additionally considering AC resistance and equivalent resistance for AC copper loss due to field excitation presented in Fig. 10(a)–(f).

Fig. 11 shows the process for optimizing the current vector for MTPA and flux-weakening control using the proposed model. The process is fundamentally same as the process presented in [29], [30], [31], [32], [33], except that the motor parameters related to the AC copper loss are additionally considered. In this article, the *d*, *q*-axis model considering only DC copper loss and iron loss in the references is defined as a conventional method. The proposed *d*, *q*-axis model has the following advantages over the conventional method.

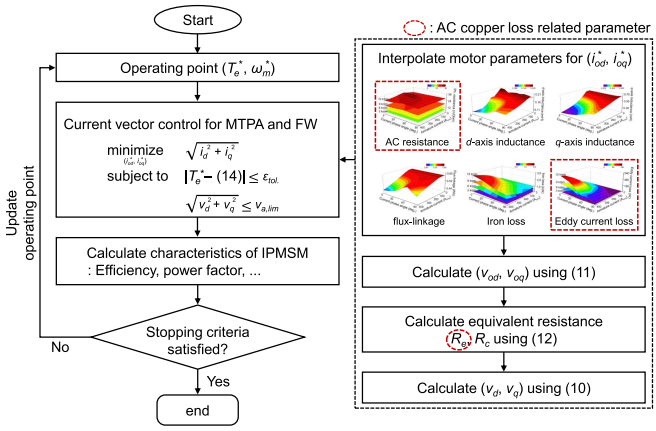

Fig. 11. Flowchart for deriving MTPA and flux-weakening characteristics of IPMSM considering AC copper loss.

1) Current vector control considering nonlinear resistive voltage drop is enabled.
2) Accurate efficiency can be derived as the AC copper loss is considered.

In addition, it is advantageous to improve the power density of IPMSM because the modulation index can be used to the maximized as it is a look-up table-based algorithm rather than a high-frequency signal injection-based algorithm.

The optimization process for the current vector is as follows. First, the motor parameters according to the current vector are interpolated using the look-up table of Fig. 10(a)–(f), in order to minimize the amplitude of current vector. Then, the electromagnetic torque and terminal voltage are calculated using the motor parameters to check whether the constraints are satisfied. When the current vector is optimized, the characteristic map of the IPMSM can be derived. The process is repeated according to all speeds and torques, and when the maximum speed is reached, the process is terminated.

In order to show the validity of proposed *d, q*-axis model, comparison with the current vector control characteristics derived using the conventional and proposed model is conducted. Fig. 12(a) shows the MTPA characteristics of IPMSM depending on whether the AC copper loss is considered. As the MTPA control is achieved in low speed than the flux-weakening control, the proportion of AC copper loss to the total loss is low. Therefore, the influence of AC resistance and eddy current loss in the MTPA region is not significant. In addition, the current vector for the target torque is not constrained by the voltage limit because the terminal voltage in MTPA region is within the limit. As a result, it can be seen that there is little difference in the MTPA trajectory between the current vector according to the electromagnetic torque calculated by using conventional and proposed method. Fig. 12(b) shows the flux-weakening characteristics of IPMSM depending on whether the AC copper loss is considered. Since the AC resistance and eddy current loss are increased due to the skin and proximity effect in high-speed region, the resistive voltage drop and *d, q*-axis currents for AC copper loss increase as the rotational speed increases. In addition, additional *d*-axis current for flux-weakening control is required because of the

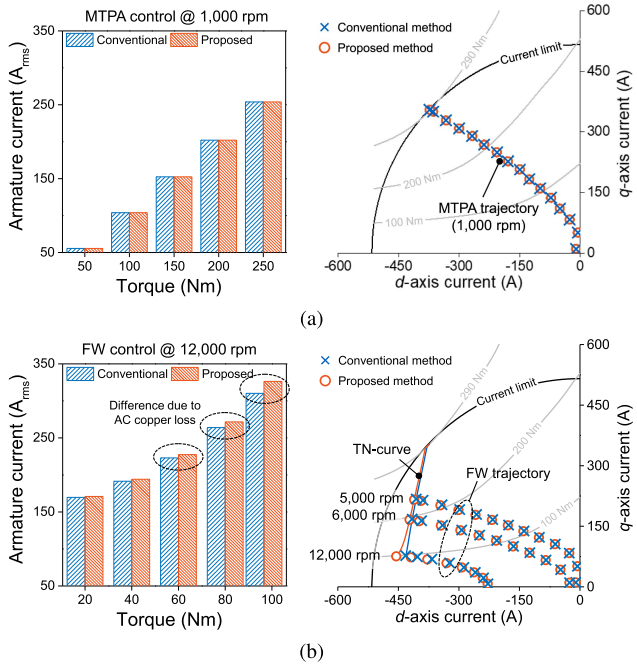

Fig. 12. *d, q*-axis current trajectory of IPMSM when the current vector is optimized for (a) MTPA and (b) flux-weakening control whether the AC copper loss is considered or not.

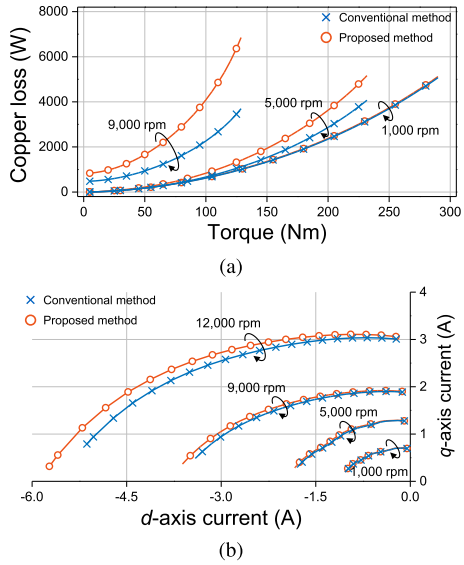

Fig. 13. Characteristics of IPMSM according to the electromagnetic torque and rotational speed whether the AC copper loss is considered or not: Trajectory of (a) copper loss and (b) *d, q*-axis current for electromagnetic loss.

increased resistive voltage drop due to the AC copper loss. As a result, it can be seen that the difference in current vectors of flux-weakening control trajectory between each result increases as the rotational speed increases.

Fig. 13(a) and (b) shows the trajectory of copper loss and *d, q*-axis currents for electromagnetic loss according to the torque and rotational speed, respectively. It can be seen that the difference in copper loss increases as the rotational speed increases shown in Fig. 13(a). This is because the AC copper loss is highly affected

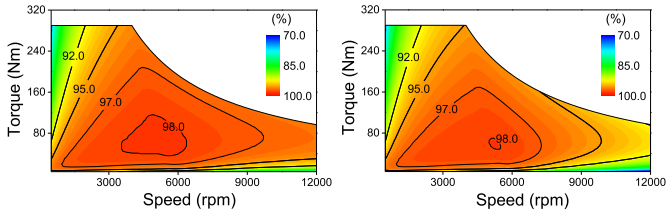

Fig. 14. Efficiency map of IPMSM according to speed and torque: (a) without considering AC copper loss, (b) with considering AC copper loss.

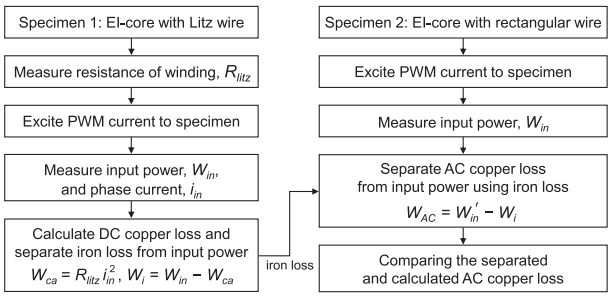

Fig. 15. Flowchart for verifying magneto-static analysis-based AC copper loss.

by the rotational speed. In addition, the *d, q*-axis currents for iron loss and AC copper loss due to field excitation are increased as the rotational speed increases also as shown in Fig. 13(b). In other words, the effect of AC copper loss is significant in high-speed region. Therefore, it is necessary to study the current vector control considering motor parameters related to the AC copper loss in analysis of traction motor with hairpin winding.

Fig. 14(a) and (b) shows the efficiency map according to whether AC copper loss is considered. Since the AC copper loss is highly dependent on the rotational speed as shown in Fig. 14(b), it can be seen that the efficiency difference is large especially in the high-speed region, where the flux-weakening control is required.

IV. Experimental Verification

In this section, experiments were conducted to verify the AC copper loss and current vector control characteristics of the IPMSM. This section consists of two parts. Experiments to verify the AC copper loss based on the magneto-static analysis are described in the first part, and experiments to verify the MTPA and flux-weakening characteristics are described in the second part.

A. Verification of AC Copper Loss Using EI-Core

The AC copper loss of electric machine is difficult to derive by conducting experiments, because the electric machine has complex magnetic circuit. Therefore, the AC copper loss of electric machine should be calculated using electromagnetic FEA. Thus, simple test for improving consistency of analysis of AC copper loss was conducted. The process for verifying the

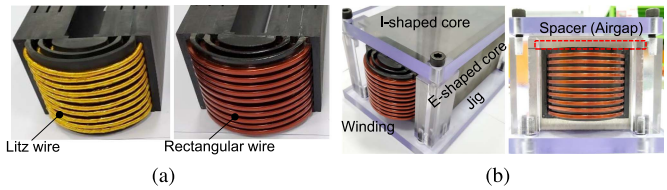

Fig. 16. Specimens for verifying AC copper loss. (a) Litz wire or rectangular wire wounded EI-core and (b) assembled EI-core for experiment.

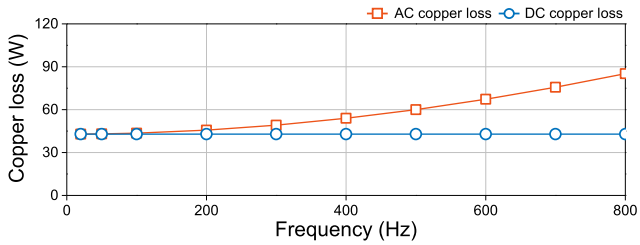

Fig. 17. Simulation results of AC copper loss for EI-core according to the frequency.

AC copper loss is shown in Fig. 15. The flowchart for conducting simple experiments is shown as follows.

The verification consists of two steps. The first step is to separate the iron loss from the input power of EI-core, and the second step is to verify the AC copper loss using the separated iron loss. In this experiments, the following assumptions were used. First, the AC copper loss is ignorable in the Litz wire. Second, iron loss of EI-core is constant under the same armature excitation and frequency. Third, there is no mechanical output because the EI-core is constrained by the mechanical components. Last, the AC copper loss consists of DC copper loss and eddy current loss in conductors.

In order to verify the AC copper loss, two EI-cores were fabricated for the experiments as shown in Fig. 16(a) and (b). The first one is wound with Litz wire to exclude the effect of skin and proximity effect. Thus, the iron loss can be separated by subtracting the DC copper loss from the input power after exciting the sinusoidal current to the Litz wire. The second one is wound with rectangular wire to consider the AC copper loss. After exciting the sinusoidal current to the rectangular wire, the AC copper loss can be derived by subtracting the separated iron loss from the input power. The verification of the AC copper loss can be performed by comparing the derived AC copper loss from the experiment with the AC copper loss calculated using magneto-static analysis-based method under the same conditions of the experiment. In order to perform the experiments according to the airgap length, the spacer of 1 or 2 mm was installed between EI-core.

Before conducting experiments, trends of AC copper loss according to the frequency is analyzed using proposed AC copper loss calculation method. Fig. 17 shows the copper loss according to the frequency of the EI-core with the airgap set to 2 mm and armature current as 30 A_{rms}. It can be seen that the AC copper loss of the specimen converges to the DC copper loss as the frequency decreases because there is no magnetic

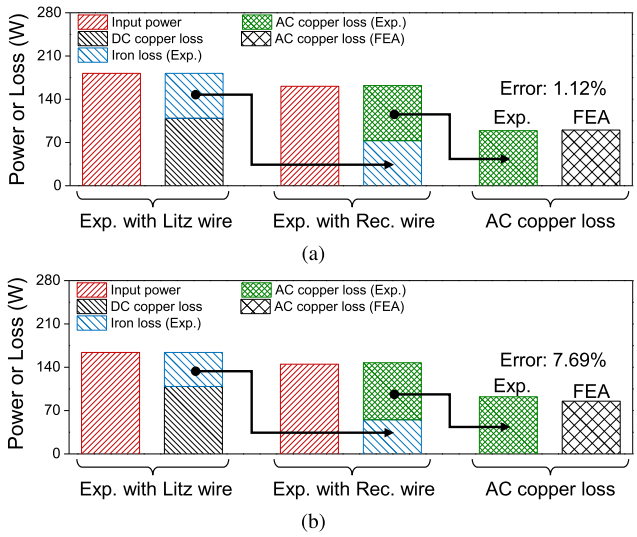

Fig. 18. Experiment results for verifying the AC copper loss when the airgap is (a) 1 mm and (b) 2 mm.

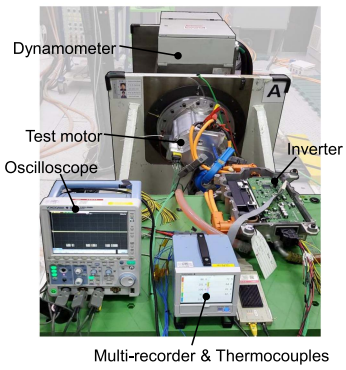

Fig. 19. Experimental setup for measuring characteristics of IPMSM.

field variation due to the PMs and no eddy current loss occurs in the conductors.

The results for comparing the separated and calculated AC copper loss are shown in Fig. 18(a) and (b). The experiments were conducted at armature current with 30 A_{rms} and 800 Hz for each airgap length. It can be seen that the errors between the simulation and experiment are less than 8%. Therefore, it is suitable to use the calculated AC copper loss in the characteristic analysis of the IPMSM.

B. Verification of MTPA and Flux-Weakening Characteristics of IPMSM Considering AC Copper Loss

Fig. 19 shows the experimental setup for measuring the characteristics of the IPMSM. A multirecorder and thermocouples were installed to monitor whether the winding temperature was maintained at an appropriate value. Fig. 20(a) and (b) shows the waveform and harmonic analysis results of line to line back-EMF at 1000 rpm. Since the difference between the simulation and test results is 2.63% based on the rms value, the specimen was properly fabricated according to the design result.

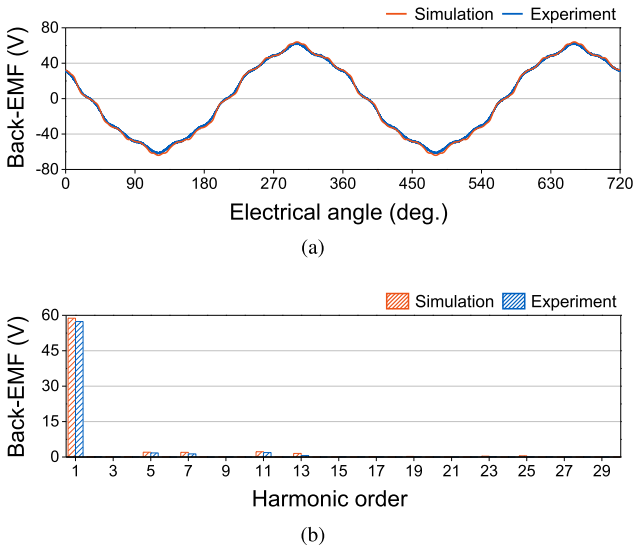

Fig. 20. Simulated and experiment results of line to line back-EMF. (a) Waveform and (b) harmonic analysis result of the back-EMF.

TABLE II
EXPERIMENTAL CONDITIONS

Index	Load torque (N·m)	Motor speed (rpm)	Vector control
Exp. 1	290	2 000	MTPA
Exp. 2	55	4 000	MTPA
Exp. 3	55	8 000	FW
Exp. 4	55	12 000	FW

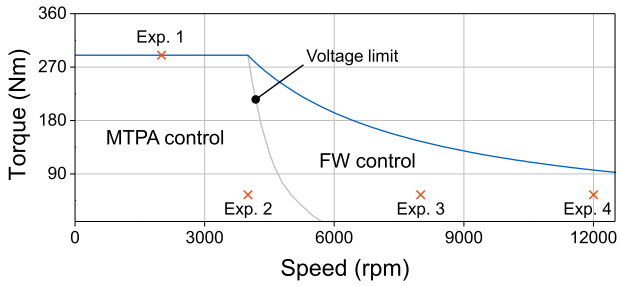

Fig. 21. Selected operating points to evaluate the effect of AC copper loss according to the current vector control.

In order to verify the validity of the proposed equivalent circuits, the load tests were conducted at the operating points listed in Table II. The experiments were performed to evaluate the effect of AC copper loss according to the current vector control by selecting total four operating points, which are two points in MTPA region and two points in flux-weakening region as shown in Fig. 21. The experiments were conducted in a state in which sufficient continuous driving for temperature equilibrium was made to exclude the influence of parameter uncertainty. The efficiency in the low-speed region under MTPA control and high-speed region under flux-weakening were measured through the experiments. Fig. 22(a) and (b) shows the comparisons of the efficiency between the simulation and experiment results at MTPA and flux-weakening control regions. The simulation results include copper loss, eddy current loss of conductors

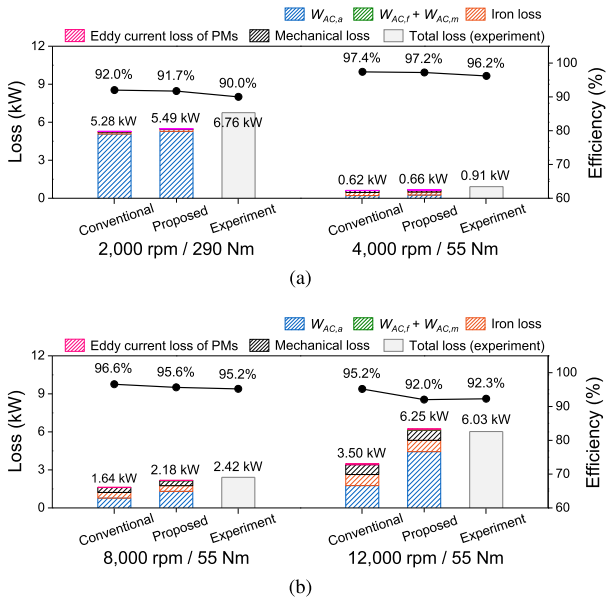

Fig. 22. Comparison of simulation and experiment results for efficiency of IPMSM at (a) MTPA control region and (b) flux-weakening control region.

and PMs, iron loss, and the mechanical loss. The mechanical loss was derived using indirect method proposed in [25] using no-load loss and electromagnetic FEA. In order to compare the simulation results with experiment results, the efficiency was calculated by considering the mechanical loss measured at each speed and eddy current loss of PMs computed with 3-D electromagnetic FEA. As a result of comparing the efficiency, it can be seen that the simulation results using the proposed equivalent circuits have less error than the others. This is because the AC copper loss, which is dependent on the armature current and rotational speed, is considered when calculating the efficiency using the proposed equivalent circuits. In addition, since the AC copper loss and armature current for electromagnetic loss for maintaining the mechanical power is increased as the rotational speed increases, the error between the experimental results and simulation results using conventional method is increased.

Therefore, the result of conventional equivalent circuits in which the AC copper loss is not considered has a large error in the high-torque or high-speed region, where the proportion of AC copper loss is large.

V. Conclusion

This article investigated AC copper loss of armature winding considering the effect of field and armature excitation. Using the proposed separation process, magnetic saturation according to current vector and AC copper loss for each component according to rotational speed were analyzed, and the method was verified to be reasonable through comparison with transient FEA. In addition, an advanced *d, q*-axis model for considering the AC copper loss was proposed. Using the proposed equivalent circuits, it is possible to calculate the current vector control characteristics of a motor which is highly influenced by the AC copper loss such as IPMSM with hairpin winding more accurately. In order to secure the validity of proposed method, experiments of AC copper loss and machine level current vector control characteristics were verified through experiments.

Since the armature windings of high power density industrial motors consists of formed winding, the proposed method can be utilized to these applications for considering skin and proximity effects. Therefore, research on sizing process for industrial motors considering the AC copper loss will be conducted based on this study. In addition, the additional electromagnetic loss such as PWM-induced loss and eddy current loss of PMs will be considered in *d, q*-axis equivalent model based on this study and the design process of IPMSM will be proposed designed considering the AC copper loss.

References

[1] Y. Yang et al., "Design and comparison of interior permanent magnet motor topologies for traction applications," *IEEE Trans. Transp. Electrific.*, vol. 3, no. 1, pp. 86–97, Mar. 2017.

[2] S. Zhou, Z. Chen, D. Huang, and T. Lin, "Model prediction and rule based energy management strategy for a Plug-in hybrid electric vehicle with hybrid energy storage system," *IEEE Trans. Power Electron.*, vol. 36, no. 5, pp. 5926–5940, May 2021.

[3] L. Shao, A. E. H. Karci, D. Tavernini, A. Sorniotti, and M. Cheng, "Design approaches and control strategies for Energy-efficient electric machines for electric Vehicles–A review," *IEEE Access*, vol. 8, pp. 116900–116913, 2020.

[4] M. Ehsani, K. V. Singh, H. O. Bansal, and R. T. Mehrjardi, "State of the art and trends in electric and hybrid electric vehicles," *Proc. IEEE*, vol. 109, no. 6, pp. 967–984, Jun. 2021.

[5] M. Popescu, J. Goss, D. A. Staton, D. Hawkins, Y. C. Chong, and A. Boglietti, "Electrical Vehicles–practical solutions for power traction motor systems," *IEEE Trans. Ind. Appl.*, vol. 54, no. 3, pp. 2751–2762, May 2018.

[6] R. Wrobel, P. H. Mellor, M. Popescu, and D. A. Staton, "Power loss analysis in thermal design of Permanent-magnet Machines–A review," *IEEE Trans. Ind. Appl.*, vol. 52, no. 2, pp. 1359–1368, Mar. 2016.

[7] S. Sridharan and P. T. Krein, "Minimization of system-level losses in VSI-Based induction motor drives: Offline strategies," *IEEE Trans. Ind. Appl.*, vol. 53, no. 2, pp. 1096–1105, Mar. 2017.

[8] X. Huang, Q. Tan, L. Li, J. Li, and Z. Qian, "Winding temperature field model considering void ratio and temperature rise of a Permanent-magnet synchronous motor with high current density," *IEEE Trans. Ind. Electron.*, vol. 64, no. 3, pp. 2168–2177, Mar. 2016.

[9] G. Volpe, M. Popescu, F. Marignetti, and J. Goss, "AC winding losses in automotive traction E-machines: A new hybrid calculation method," in *Proc. IEEE Int. Electric Machines Drives Conf.*, 2019, pp. 2115–2119.

[10] G. Berardi and N. Bianchi, "Design guideline of an AC hairpin winding," in *Proc. XIII Int. Conf. Elect. Machines*, 2018, pp. 2444–2450.

[11] C. Du-Bar, A. Mann, O. Wallmark, and M. Werke, "Comparison of performance and manufacturing aspects of an insert winding and a hairpin winding for an automotive machine application," in *Proc. 8th Int. Electric Drives Prod. Conf.*, 2018, pp. 1–8.

[12] M. S. Islam, I. Husain, A. Ahmed, and A. Sathyan, "Asymmetric bar winding for high-speed traction electric machines," *IEEE Trans. Transp. Electrific.*, vol. 6, no. 1, pp. 3–15, Mar. 2019.

[13] J.-W. Chin, K.-S. Cha, M.-R. Park, S.-H. Park, E.-C. Lee, and M.-S. Lim, "High efficiency PMSM with high slot fill factor coil for heavy-duty EV traction considering AC resistance," *IEEE Trans. Energy Convers.*, vol. 36, no. 2, pp. 883–894, Jun. 2021.

[14] K.-S. Cha, J.-W. Chin, S.-H. Park, Y.-H. Jung, E.-C. Lee, and M.-S. Lim, "Design method for reducing AC resistance of traction motor using high fill factor coil to improve fuel economy of eBus," *IEEE/ASME Trans. Mechatron.*, vol. 26, no. 3, pp. 1260–1270, Jun. 2021.

[15] C. Du-Bar and O. Wallmark, "Eddy current losses in a hairpin winding for an automotive application," in *Proc. XIII Int. Conf. Elect. Machines*, 2018, pp. 710–716.

[16] T. Jokinen, V. Hrabovcova, and J. Pyrhonen, *Design of Rotating Electrical Machines*. New York, NY, USA: Wiley, 2013.

[17] L. Wu and Z. Zhu, "Simplified analytical model and investigation of open-circuit AC winding loss of permanent-magnet machines," *IEEE Trans. Ind. Electron.*, vol. 61, no. 9, pp. 4990–4999, Sep. 2013.

[18] A. Bardalai et al., "Reduction of winding AC losses by accurate conductor placement in high frequency electrical machines," *IEEE Trans. Ind. Appl.*, vol. 56, no. 1, pp. 183–193, Jan. 2019.
[19] H. Sugimoto, Y. Yamada, and K. Imae, "Analysis of winding AC loss in a permanent magnet synchronous machine with high slot fill aluminum winding," in *Proc. Int. Power Electron. Conf.*, 2022, pp. 2741–2745.
[20] J.-W. Chin, Y.-H. Jung, J.-Y. Ryu, M.-R. Park, and M.-S. Lim, "Computationally cost-efficient characteristics analysis of EV traction motor considering AC copper loss based on 2-D magneto-static analysis," in *Proc. Int. Conf. Elect. Machines*, 2020, pp. 1723–1729.
[21] N. Taran, D. M. Ionel, V. Rallabandi, G. Heins, and D. Patterson, "An overview of methods and a new three-dimensional FEA and analytical hybrid technique for calculating AC winding losses in PM machines," *IEEE Trans. Ind. Appl.*, vol. 57, no. 1, pp. 352–362, Jan.–Feb. 2020.
[22] A. Fatemi, D. M. Ionel, N. A. Demerdash, D. A. Staton, R. Wrobel, and Y. C. Chong, "Computationally efficient strand eddy current loss calculation in electric machines," *IEEE Trans. Ind. Appl.*, vol. 55, no. 4, pp. 3479–3489, Jul. 2019.
[23] J.-W. Chin, K.-S. Cha, J.-C. Park, D.-M. Kim, J.-P. Hong, and M.-S. Lim, "Investigation of AC resistance on winding conductors in slot according to strands configuration," *IEEE Trans. Ind. Appl.*, vol. 57, no. 1, pp. 316–326, Jan. 2020.
[24] S. Kawahara, K. Umetani, and E. Hiraki, "Analysis and Prediction of AC Resistance of Litz Wire With Rectangular Cross-Section," in *Proc. IEEE Energy Convers. Congr. Expo.*, 2020, pp. 3273–3279.
[25] S.-H. Park, E.-C. Lee, J.-C. Park, S.-W. Hwang, and M.-S. Lim, "Prediction of mechanical loss for high power density PMSM considering eddy current loss of PMs and conductors," *IEEE Trans. Magn.*, vol. 57, no. 2, Feb. 2021.
[26] Z. Azar, Z. Zhu, and G. Ombach, "Influence of electric loading and magnetic saturation on cogging torque, back-EMF and torque ripple of PM machines," *IEEE Trans. Magn.*, vol. 48, no. 10, pp. 2650–2658, Oct. 2012.
[27] S.-H. Park, J.-W. Chin, K.-S. Cha, J.-Y. Ryu, and M.-S. Lim, "Characteristic analysis of IPMSM for EV traction considering the effect of field and armature excitations on AC copper loss," in *Proc. IEEE Energy Convers. Congr. Expo.*, pp. 4486–4491, 2021.
[28] J. Pyrhonen, T. Jokinen, and V. Hrabovcova, *Design of Rotating Electrical Machines*. New York, NY, USA: Wiley, 2013.
[29] Y. Zhang, K. Liu, Y. Hu, and S. Yang, "MTPA control of IPMSM with aiding from estimation of dq-axis inductances," in *Proc. IEEE Student Conf. Elect. Mach. Syst.*, 2018, pp. 1–5.
[30] S. Kim, Y.-D. Yoon, S.-K. Sul, and K. Ide, "Maximum torque per ampere (MTPA) control of an IPM machine based on signal injection considering inductance saturation," *IEEE Trans. Power Electron.*, vol. 28, no. 1, pp. 488–497, Jan. 2012.
[31] K. Li and Y. Wang, "Maximum torque per ampere (MTPA) control for IPMSM drives based on a variable-equivalent-parameter MTPA control law," *IEEE Trans. Power Electron.*, vol. 34, no. 7, pp. 7092–7102, Jul. 2018.
[32] T. Sun, J. Wang, and M. Koc, "On accuracy of virtual signal injection based MTPA operation of interior permanent magnet synchronous machine drives," *IEEE Trans. Power Electron.*, vol. 32, no. 9, pp. 7405–7408, Sep. 2016.
[33] Q. Chen, W. Zhao, G. Liu, and Z. Lin, "Extension of virtual-signal-injection-based MTPA control for five-phase IPMSM into fault-tolerant operation," *IEEE Trans. Ind. Electron.*, vol. 66, no. 2, pp. 944–955, Feb. 2018.

Soo-Hwan Park received the bachelor's degree in mechanical engineering and the Ph.D. degree in automotive engineering from Hanyang University, Seoul, South Korea, in 2014 and 2022, respectively.

From 2019 to 2020, he was with the Korea Institute of Industrial Technology, South Korea. Since 2022, he has been with the R&D Division of Hyundai Motor Company, South Korea, where he is currently a Senior Research Engineer. His research interests include electromagnetic field analysis, design, and optimization of electric machines for automotive and robotics applications, and thermal management system for electric vehicles.

Jun-Woo Chin received the bachelor's degree in mechanical engineering from Hanyang University, Seoul, South Korea, in 2014, the integrated master's and Ph.D. degree in automotive engineering from Hanyang University, Seoul, in 2022.

Since 2022, he has been with Future Powertrain Technologies Research Laboratory of Korea Automotive Technology Institute (KATECH), Cheonan, South Korea, where he is currently a Senior Engineer. His research interests are electromagnetic field, loss, multiphysics analysis of electric machines, and their design optimization considering systems such as automotive application.

Kyoung-Soo Cha received the bachelor's degree in electric engineering from Chungbuk University, Cheongju, South Korea, in 2015, the Ph.D. degree in automotive engineering from Hanyang University, Seoul, South Korea, in 2022.

In 2022, he was a Postdoctoral Researcher with Hanyang University, Seoul. Since 2022, he has been with Korea Institute of Industrial Technology, Daegu, South Korea, where he is currently Postdoctoral Researcher. His research interests are electric machine design for automotive and home appliance, system modeling and optimization of electric vehicles, hybrid electric vehicle, and fuel cell electric vehicles.

Jun-Yeol Ryu received the bachelor's degree in mechanical engineering and electronic systems engineering from Hanyang University, Ansan, South Korea, in 2016. He is currently working toward the Ph.D degree in automotive engineering with Hanyang University, Seoul, South Korea.

His research interests include design and optimization of electric machines and analysis of electro-magnetic field.

Myung-Seop Lim (Member, IEEE) received the bachelor's degree in mechanical engineering and the master's and Ph.D. degrees in automotive engineering from Hanyang University, Seoul, South Korea, in 2012, 2014, and 2017, respectively.

From 2017 to 2018, he was a Research Engineer in Hyundai Mobis, Yongin, South Korea. From 2018 to 2019, he was an Assistance Professor with Yeungnam University, Daegu, South Korea. Since 2019, he has been with Hanyang University, Seoul, where he is currently an Assistant Professor. His research interests include electromagnetic field analysis and electric machinery for mechatronics systems such as automotive and robot applications.